Fracture Process of Microgel–Reinforced Hydrogels under Uniaxial Tension

ARTICLE *in* MACROMOLECULES · MAY 2014

Impact Factor: 5.8 · DOI: 10.1021/ma5008545

6 AUTHORS, INCLUDING:

Jhen-Jia Hu
National Taiwan University
317 PUBLICATIONS **6,285** CITATIONS
SEE PROFILE

Zi Liang Wu
Zhejiang University
29 PUBLICATIONS **459** CITATIONS
SEE PROFILE

Macromolecules

Article

pubs.acs.org/Macromolecules

Fracture Process of Microgel-Reinforced Hydrogels under Uniaxial Tension

Jian Hu,[†] Takayuki Kurokawa,[‡] Tasuku Nakajima,[‡] Zi Liang Wu,[†] Song Miao Liang,[‡] and Jian Ping Gong*[,‡]

[†]Graduate School of Science, Hokkaido University, Sapporo 060-0810, Japan

[‡]Faculty of Advanced Life Science, Hokkaido University, Sapporo 060-0810, Japan

ABSTRACT: We have found that lightly cross-linked neutral hydrogels containing microgels of densely cross-linked polyelectrolyte show high strength and toughness. These kinds of hydrogels, named as microgel-reinforced (MR) hydrogels, are a two-phase composite, where the disperse phase is the microgel with the double network (DN) structure and the continuous phase is the soft neutral gel matrix. The brittle polyelectrolyte network of the DN microgels, though in disperse phase, also serves as sacrificial bonds to toughen the material, similar to conventional DN gels. In this paper, we study the internal fracture process of the MR gel under uniaxial tension. The tensile stress−strain curve of the MR gel is charaterized by four regions according to its differential curve: elastic region ($0 < \varepsilon < 1$), preyielding region ($1 < \varepsilon < 3$), yielding region ($3 < \varepsilon < 7$), and strain hardening region ($\varepsilon > 7$). The morphology change of microgels in the reswollen MR gels after prestretching tells that the internal fracture of microgels, which occurs beyond the elastic region ($\varepsilon > 1$), is anisotropic. That is, the short chains in the tensile direction fracture first ($1 < \varepsilon < 3$); at large stretching, both the long chains in the tensile direction and the short chains in the transverse direction fracture ($3 < \varepsilon < 7$), followed by the fracture of the long chains in the transverse direction ($\varepsilon > 7$). These anisotropic fracture behaviors are in similar to bulk DN gels. Moreover, at each stage of the tensile process, large microgels always fracture *prior to* small ones and own higher fracture efficiency in the chain rupture than the smaller ones. This size effect is attributed to the stress concentration effect around the two poles of large microgels induced by the close distance from their neighboring microgels.

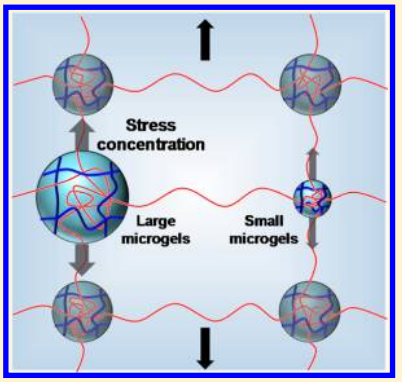

INTRODUCTION

In the past decade, a variety of hydrogels with improved mechanical strength and toughness have been developed.[1−3] Double network hydrogels (DN gels), which are as tough as load-bearing cartilages and filled rubbers, are the toughest synthetic hydrogels with a high modulus.[4−6] Extensive studies on the toughening mechanism of DN gels, consisting of highly cross-linked polyelectrolyte as the first network and lowly cross-linked neutral polymer as the second network, have shown that the enhanced toughness of DN gels is due to the internal fracture of the brittle first network, which effectively dissipates energy and increases the resistance against the crack propagation.[7−9] The ductile second network gives rise to the rupture of the first network over a large zone through their mutual entanglement.[10,11] The studies on DN gels suggest that introduction of any effective *sacrificial bonds* that rupture to show Mullins effect upon deformation will toughen the materials. Based on this concept, various motifs of sacrificial bonds have been designed for the enhancement of hydrogels.[12−27]

One successful approach is to use densely cross-linked microgels as *sacrificial bonds* to replace the densely cross-linked polyelectrolyte macronetwork for conventional DN hydrogels.[28−30] These hydrogels, named as microgel-reinforced hydrogels (MR gels), were prepared by synthesizing neutral hydrogels from the precursor monomer solution containing a certain amount of microgels. Our previous studies have shown that the strength and toughness of sparsely cross-linked neutral polyacrylamide (PAAm) hydrogels containing densely cross-linked polyelectrolyte microgels of poly(sodium 2-acrylamido-2-methylpropanesulfonate) (PNaAMPS) are comparable to those of the conventional bulk DN gels at their optimal formulation, where the volume fraction of dispersion occupied by microgels and the molar ratio of the AAm monomer to the NaAMPS monomer in the microgel phase are two critical parameters governing the toughness of the gels.[29]

This MR gel approach has many advantages over the conventional DN gel approach in practical applications. (1) In the MR gel approach, the precursor is solution, and it is easy to handle in comparison with the very fragile first network of DN gels. (2) Loading of the second network monomer in the microgels is very fast since the diffusion time scales with the size in square. (3) MR gels are conformable to various shape formations since they are synthesized via a one-step solidification process. Besides the above advantages in sample preparation, MR gels have additional advantages over conven-

Received: April 24, 2014
Revised: May 18, 2014

   dx.doi.org/10.1021/ma5008545 | *Macromolecules* XXXX, XXX, XXX−XXX

tional DN gels when they are used as load-bearing tissue scaffolds. For example, the loose network structure in the matrix phase of MR gels favors the smooth mass transportation process and therefore facilitates a high cell viability and good biological behaviors.[31] As the MR gels are promising for various practical applications, understanding of the toughening mechanism of this system is greatly meaningful.

MR gels can be regarded as a two-phase composite, where the disperse phase is the *rigid* DN microgels and the continuous phase is the *soft* PAAm matrix. We have demonstrated that the high mechanical strength and toughness of MR gels originate from the internal fracture of PNaAMPS microgels, similar to the fracture mechanism of DN gels. Further, we have found that the DN microgels embedded in MR gels show 4 times higher fracture efficiency of the sacrificial bonds than the bulk DN gels at the same strain, as a result of the stress concentration around the two poles of microgels.[30] These previous studies further raise many open questions. For example, why does the internal fracture occur in the dispersed DN microgel phase but not in the continuous PAAm phase? How does the fracture occur? Is there any size effect of microgels in the fracture process for the wide size distribution of microgels? Answering these questions will enable us to understand the underlying toughening mechanism of MR gels and benefit from the optimization of this novel approach.

To address some of these questions, in this paper, we quantitatively analyze the morphology of microgels after the uniaxial stretching through optical observation. To analyze anisotropic internal fracture, we use reswollen samples after prestretching, taking the advantage that DN gels show additional swelling by internal fracture.[32] On the basis of the size and shape changes of the microgels, we elucidate the intrinsic correlation between the stress−strain mechanical response and the microscopic internal fracture of microgels as well as the size effect of microgels.

EXPERIMENTAL SECTION

Materials. The monomer sodium 2-acrylamido-2-methylpropanesulfonate (NaAMPS) (Tokyo Kasei Co., Ltd.) was used as received. The cross-linker *N,N′*-methylenebis(acrylamide) (MBAA) (Tokyo Kasei Co., Ltd.) was recrystallized from ethanol. The monomer acrylamide (AAm) (Junsei Chemical Co., Ltd.) was recrystallized from chloroform. The UV initiator 2-oxoglutaric acid (OA) (Wako Pure Chemical Industries, Ltd.) was used as received. The surfactant polyglycerol polyricinoleate (PGPR) (Danisco Co., Ltd.) was used as received. The solvent kerosene (Wako Pure Chemical Industries, Ltd.) was used as received. The dye Alcian Blue (Wako Pure Chemical Industries, Ltd.) was used as received. Milli-Q (18.3 MΩ) water was used in all experiments.

Synthesis. *Preparation of Microgels.* PNaAMPS microgels were prepared by SPG (Shirasu Porous Glass) membrane emulsification and UV polymerization. First, water/oil (W/O) emulsion was prepared by a high-speed mini kit equipped with a hydrophobic SPG membrane (SPG Technology Co., Ltd.). The disperse phase was an aqueous solution of 1 M NaAMPS containing 4 mol % cross-linker MBAA and 0.1 mol % UV initiator OA with respect to NaAMPS monomer. The disperse phase, stored in a pressure-tight vessel, was pressed into the continuous phase, kerosene containing 1 wt % surfactant PGPR, through the hydrophobic SPG membrane (pore diameter = 4.9 μm) under argon transmembrane pressure of 14 kPa. After being bubbled with argon for 1 h, the W/O emulsion was irradiated at 365 nm UV with intensity of 4 mW/cm^2 under an argon atmosphere for 8 h to get polymerized microgels. To purify the PNaAMPS microgels, they were precipitated with acetone to remove the surfactant, then reswollen in deionized water to remove the residual monomers, and finally separated by ultracentrifugation at 10^4 rpm for three times. After freeze-drying, the dried PNaAMPS microgels were obtained as fine powders.

Preparation of MR Hydrogels. 0.07 g of dried PNaAMPS microgel powders was swollen in 1 mL of the first aqueous precursor solution containing 2 M AAm, 0.01 mol % MBAA, 0.01 mol % OA, and 4 M sodium chloride (NaCl); here mol % was related to AAm monomer concentration. The NaCl was used to control the solution at a suitable operating viscosity. After equilibrium swelling, the pastelike solution was poured into a mold consisting of a 100 μm silicone spacer sandwiched by two parallel glass plates and then polymerized under an argon atmosphere with UV irradiation for 8 h. The as-prepared hydrogels were desalinated completely in deionized water and then swollen in the second aqueous precursor solution of 4 M AAm containing 0.01 mol % MBAA and 0.01 mol % OA. After equilibrium swelling, the swollen gels were covered by two parallel glass plates and wrapped by plastic film and then irradiated with UV under an argon atmosphere for 8 h. Finally, the gels were swollen in deionized water to remove the residual chemicals, and the tough MR gels with two interpenetrating PAAm networks were obtained.

Characterizations. *Tensile Test.* Tensile test was performed with a commercial test machine (Tensilon RTC-1150A, Orientec Co.). Fully swollen samples were cut into a dumbbell shape as standardized JIS-K6251-7 sizes (length 35 mm, width 2 mm, gauge length 12 mm) with a gel cutting machine (DumbBell Co., Ltd.). Both ends of the dumbbell-shaped samples were clamped and stretched at a constant velocity of 100 mm/min, by which the stress−strain curves were recorded.

Selective Dyeing of MR Gels. To visualize the microgels embedded in MR gels, MR gels were immersed in 3 vol % acetic acid aqueous solution containing 1 wt % Alcian Blue for 15 min and then washed by copious deionized water. The tetravalent cationic Alcian Blue dyes the anionic PNaAMPS microgels selectively, but not the neutral PAAm matrix, which produces a sharp contrast between the microgel phase and the matrix phase in favor of the observation of microgels under an optical microscope.

Size Distribution of Microgels in MR Gels. To characterize the size distribution of PNaAMPS microgels in MR gels, their micrographs were captured under an optical microscope and were analyzed by Image-Pro Plus. The size distribution of the microgels was determined by statistically measuring the diameter d_0 of 100 microgels. The average diameter of the microgels in the intact MR gels, D_0, is estimated from the average of 100 microgels.

$$D_0 = \sum_{i=1}^{100} d_{0,i}/100 \tag{1}$$

Here $d_{0,i}$ is the diameter of the ith microgel in the intact MR gels. When MR gels experience tensile deformation at various maximum strain ε_{max} and are immersed in deionized water, the embedded microgels swell due to the internal fracture of PNaAMPS microgels. The swollen microgels exhibit an ellipsoidal shape with the major axis of c and the minor axis of a due to anisotropic internal fracture. The size of each individual ellipsoid is characterized by the equivalent diameter d of its isovolume sphere, determined as follows:

$$d = \sqrt[3]{a^2 c} \tag{2}$$

The mean equivalent diameter D_m corresponding to a certain ε_{max} is estimated by averaging 100 statistically selected ellipsoids with the equivalent diameter d.

$$D_m = \sum_{i=1}^{100} d_i/100 \tag{3}$$

Here d_i is the equivalent diameter of the ith microgel estimated from eq 2. The coefficient of variation CV, defined as CV = (SD/D_m) × 100%, where SD is the standard deviation of D_m, is used to evaluate the dispersion of the size distribution of microgels.

Volume Expansion Ratio. After experiencing tensile deformation at different maximum strain ε_{max} and reswelling in water, the dumbbell MR gels increase their gauge length, width, and thickness from the

dx.doi.org/10.1021/ma5008545 | Macromolecules XXXX, XXX, XXX−XXX

initial values before deformation l_0, w_0, t_0 to l, w, t, respectively. Meanwhile, the embedded microgels also expand in volume. Since $d_{0,i}$ and d_i could not be obtained from the same microgel, we could not discuss the expansion ratio of each specific microgel. Instead, we discuss the correlation between their average values of D_0 and D_m. The *global* volume expansion ratio of bulk MR gels Q_{MR} and the *mean* local volume expansion ratio of the embedded microgels $Q_{microgel}$ are estimated as follows:

$$Q_{MR} = \frac{lw^2}{l_0 w_0^2} \tag{4}$$

$$Q_{microgel} = \left(\frac{D_m}{D_0}\right)^3 \tag{5}$$

Here, $l/l_0 \neq w/w_0 = t/t_0$ due to anisotropic fracture.

Swelling Anisotropy. The swelling anisotropy of bulk MR gels, Γ_{MR}, and of each *individual* microgel, γ, are estimated as follows:

$$\Gamma_{MR} = \frac{l/l_0}{w/w_0} \tag{6}$$

$$\gamma = \frac{c/d}{a/d} = \frac{c}{a} \tag{7}$$

The mean swelling anisotropy $\Gamma_{microgel}$ of microgels is estimated by averaging 100 microgels:

$$\Gamma_{microgel} = \sum_{i=1}^{100} \gamma_i/100 \tag{8}$$

Here γ_i is the swelling anisotropy of the ith microgel estimated from eq 7.

RESULTS AND DISCUSSION

Fracture Process of Microgels in MR Gels under Uniaxial Tension. As have been clarified by the previous studies, the stress−strain curve of DN gels has three well-defined regions, separated by the yield point and the strain hardening point, as preyielding region ($0 < \varepsilon < 2$), yielding region ($2 < \varepsilon < 10$), and hardening region ($\varepsilon > 10$).[7,10,32] In contrast, a MR gel does not show distinct yield point and strain hardening point in its stress−strain curve (Figure 1). As the soft PAAm network is the continuous phase, the initial modulus of a MR gel is softer than its corresponding DN gel.

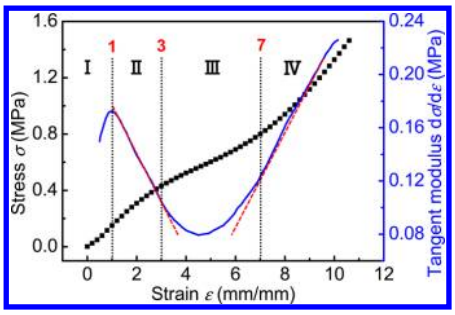

Figure 1. Tensile stress−strain curve of MR gels (black square dots). The blue curve is the differential curve corresponding to the tensile stress−strain curve (points of window = 600), as an indication of the tangent modulus $d\sigma/d\varepsilon$. From the behavior of the tangent modulus $d\sigma/d\varepsilon$, the differential curve is divided into four regions, as elastic region (I: $0 < \varepsilon < 1$), preyielding region (II: $1 < \varepsilon < 3$), yielding region (III: $3 < \varepsilon < 7$), and strain hardening region (IV: $\varepsilon > 7$). The red dashed lines are guides to the eye for the linear decrease (II) and increase (IV) of $d\sigma/d\varepsilon$.

To elaborate the nonlinear mechanical response of the MR gel during elongation, we plotted the differential curve corresponding to the stress−strain curve in Figure 1, as an indication of the tangent modulus $d\sigma/d\varepsilon$. On the basis of the mechanical behavior of $d\sigma/d\varepsilon$, we divided the stress−strain curve of MR gels into four regions: (I) elastic region ($0 < \varepsilon < 1$), where $d\sigma/d\varepsilon$ increases linearly with ε; (II) preyielding region ($1 < \varepsilon < 3$), where $d\sigma/d\varepsilon$ decreases abruptly; (III) yielding region ($3 < \varepsilon < 7$), where $d\sigma/d\varepsilon$ decreases slowly, reaches a minimum at $\varepsilon = 5$, and then increases gradually beyond $\varepsilon = 5$; (IV) hardening region ($\varepsilon > 7$), where $d\sigma/d\varepsilon$ increases sharply until the ultimate failure. We will show later that the feature of these four regions results from the different fracture behaviors of microgels.

In the previous work,[30] through *in situ* observation of MR gels during the uniaxial tensile process, the quantitative relationship between the local average strain of microgels $\varepsilon_{microgel}$ and the global strain of MR gels ε_{MR} have been investigated. Two distinct strain regions with a boundary at the yield strain of $\varepsilon_{MR} = 3$ have been observed. In the range $0 < \varepsilon_{MR} < 3$, $\varepsilon_{microgel}$ increases weakly with ε_{MR}, with a relation of $\varepsilon_{microgel} = 0.2\varepsilon_{MR}$. When $\varepsilon_{MR} > 3$, $\varepsilon_{microgel}$ increases rapidly with ε_{MR}, with a relation of $\varepsilon_{microgel} = 1.18\varepsilon_{MR} - 2.86$. In addition, the study on the cyclic tensile test of MR gels showed that hysteresis starts to appear at $\varepsilon_{MR} = 1$, and it rapidly increases with the strain at $\varepsilon_{MR} > 1$. These results indicate that the MR gel is stretched elastically at $0 < \varepsilon_{MR} < 1$, and substantial internal fracture occurs at $\varepsilon_{MR} > 1$.

Swelling equilibrium of DN microgels is achieved by the balance between the elastic stress of PNaAMPS network and the osmotic pressure from PNaAMPS chains, dissociated counterions, and constrained PAAm chains. Any fracture of PNaAMPS network in one dimension will result in its additional swelling to a higher extent in the same dimension due to the release of the osmotic pressure. Therefore, the reswelling measurement, which has been successfully used to study the intenral fracture of DN gels,[32] is promising to provide more microscopic fracture details of MR gels corresponding to the four regions for the stress−strain response. Figure 2a shows the macroscopic dumbbell-shaped MR gels in the intact state ($\varepsilon_{max} = 0$) and in the reswollen state after experiencing a maximum strain ε_{max} of 11. The reswollen MR gel shows a prominent increase in the gauge length in comparison with the intact one, which results from the swelling release of the constrained PAAm network induced by the breakage of PNaAMPS microgels. Figure 2b shows the optical images of reswollen MR gels after subjecting to elongation at various ε_{max}. With the naked eye, we can identify that the microgels enlarge in their size and change the shape from sphere to ellipsoid with the increase in ε_{max}. The size of the ellipsoids is characterized by the mean equivalent diameter D_m. As shown in Figure 2c, the microgels enlarge notably from the initial D_0 of 7.12 μm to the final D_m of 10.84 μm with the increased ε_{max} from 0 to 11. Moreover, the corresponding coefficient of variation CV at various ε_{max} remains constant as ~25%, which indicates that the statistical method based on image analysis is credible. These results are in good agreement with our previous work, which shows an initial D_0 of 6.67 μm and CV of 26.3%, analyzed from the differential interference contrast (DIC) micrograph of MR gels.[29]

Generally speaking, the size increment of MR gels may come from two contributions. One is from the microgel phase due to the swelling release of the constrained PAAm network after the

dx.doi.org/10.1021/ma5008545 | Macromolecules XXXX, XXX, XXX−XXX

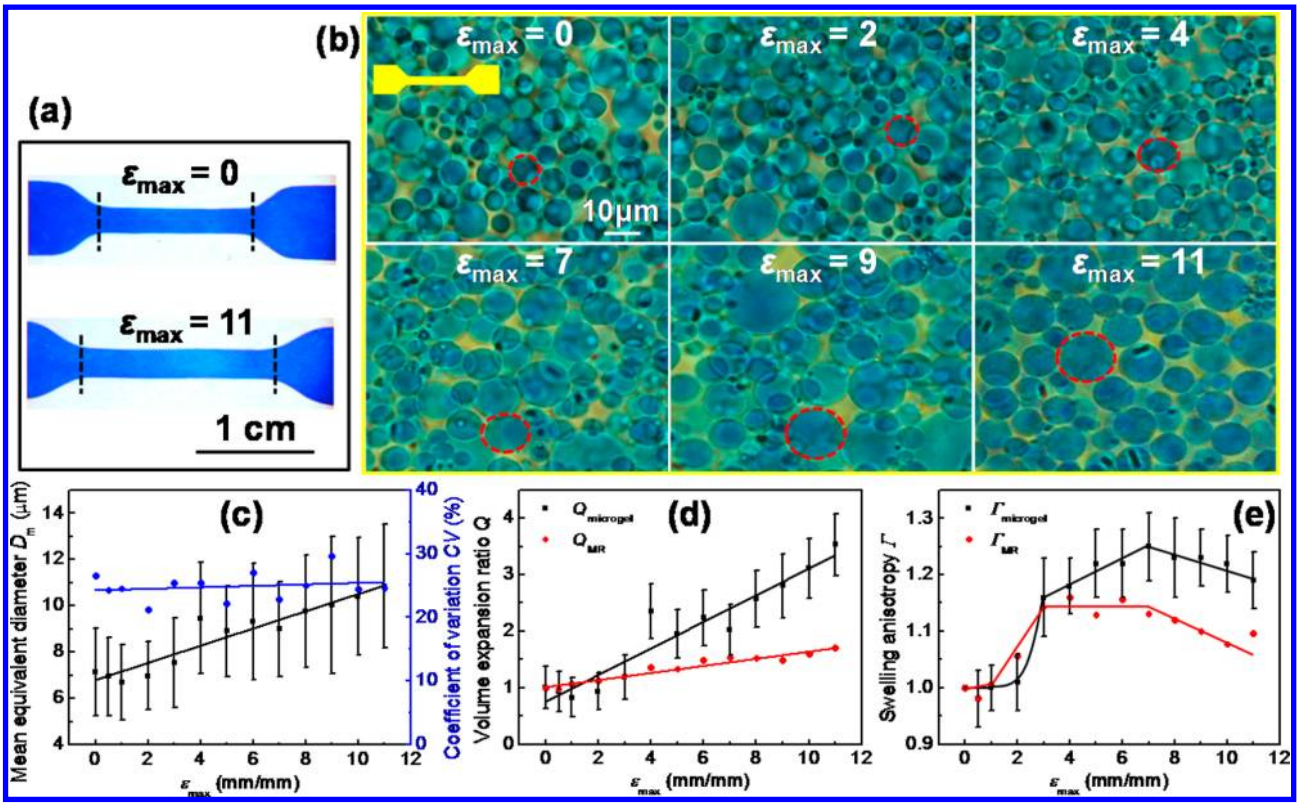

Figure 2. (a) Photo images of a dumbbell-shaped MR gel in the intact state and in the reswollen state after experiencing a maximum strain ε_{max} of 11. The gauge length is marked by the dashed lines. (b) Morphology observation of reswollen MR gels under an optical microscope. MR gels underwent tensile internal fracture at various ε_{max}. The red dashed circles profile the ellipsoidal microgels, indicating the anisotropic residual strain due to internal fracture of MR gels. (c) Mean equivalent diameter D_m and coefficient of variation CV as a function of ε_{max} for microgels in the reswollen MR gels. (d) Comparison of volume expansion ratio Q as a function of ε_{max} between bulk MR gels and the microgels in the MR gels. (e) Comparison of swelling anisotropy Γ as a function of ε_{max} between bulk MR gels and microgels. The solid lines in (c–e) are guides to the eye. All the microgel quantities are the mean values of 100 microgels in one MR gel.

breakage of PNaAMPS chains, and the other is from the matrix phase of the PAAm network due to its possible damage. As shown in Figure 2d, both $Q_{microgel}$ and Q_{MR} increase monotonously with ε_{max}. However, $Q_{microgel}$ is much larger than Q_{MR} at high ε_{max}, which indicates that the size increment of MR gels results from the fracture of the microgels phase, rather than from the fracture of the PAAm matrix phase. The result in Figure 2d is in agreement with the previous study on the cyclic tensile test of MR gels which showed that irreversible hysteresis appears at strain >1.[30] So the reswelling data in Figure 2d provides additional strong evidence to support the previously proposed argument that the high strength and toughness of MR gels root in the sacrificial bonds of the embedded microgels.[30]

In the uniaxial elongation process of MR gels, the fracture extent of microgels is different in the axial and transverse directions, which is characterized by the swelling anisotropy Γ, as shown in Figure 2e. The behavior of $\Gamma_{microgel}$ could be divided into four regions, consistent with that shown in Figure 1. $\Gamma_{microgel}$ remains constant in the elastic region ($0 < \varepsilon_{max} < 1$), increases sharply in the preyielding region ($1 < \varepsilon_{max} < 3$), then increases modestly in the yielding region ($3 < \varepsilon_{max} < 7$), and finally decreases slowly in the hardening region ($\varepsilon_{max} > 7$). This anisotropic chain rupture process of microgels in MR gels resembles that of bulk DN gels[32] and is related to the heterogeneous structure of the PNaAMPS network of the microgels. Because of the photoinitiated radical polymerization, the microgel network of PNaAMPS should be very heterogeneous with a wide distribution of chain length, the same as that of the bulk PNaAMPS hydrogel.[33] In general, the PNaAMPS chains are in random distribution, and the axially aligned chains tend to fracture in order of increasing chain length during the uniaxial tensile process. For simplicity, we adopt a bimodal chain-length distribution composed of short chain and long chain to describe the chain-length-dependent fracture process below. In the initial state of elongation, the stress mainly concentrates on the axial short chains of the microgels, which contribute to most of the elastic modulus. After the rupture of short chains, long chains start to subject to the stress sequentially.[8,32] It is worth noting that the fracture of the axial chains will increase $\Gamma_{microgel}$, while that of the transverse chains will decrease $\Gamma_{microgel}$. Therefore, Figure 2e corresponds to the chain rupture process as follows. No chain rupture occurs in I region; the axial short chains fracture in II region; the axial long chains and the transverse short chains fracture in III region; the transverse long chains fracture in IV region. This fracture process of microgels is schematically illustrated in Figure 3.

In addition, Γ_{MR} varys with ε_{max} in a similar trend as $\Gamma_{microgel}$, also including four well-defined regions, which indicates that the anisotropic swelling of MR gels is dominated by the anisotropic internal fracture of microgels completely. However, we note that the anisotropy of MR gels is the same as that of microgels ($\Gamma_{MR} = \Gamma_{microgel}$) at $\varepsilon_{max} < 3$ but smaller than that of the microgel ($\Gamma_{MR} < \Gamma_{microgel}$) at $\varepsilon_{max} > 3$. Both the residual deformation of the matrix phase and the microgel phase will

dx.doi.org/10.1021/ma5008545 | Macromolecules XXXX, XXX, XXX–XXX

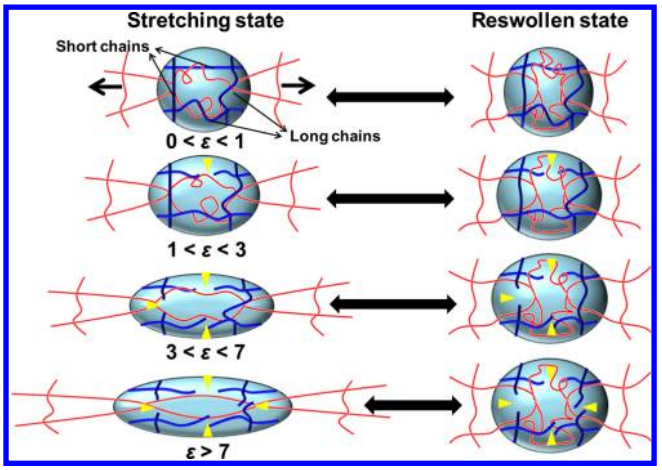

Figure 3. Schematic illustration of internal fracture process and the morphology of microgels embedded in MR gels in their stretching state and the corresponding reswollen state after prestretching. The blue and red lines stand for the PNaAMPS chains and PAAm chains, respectively. The network of PNaAMPS microgel is simply illustrated by four kinds of typical chains, as the short and long chains in the axial and transverse directions, respectively, which rupture sequentially upon elongation (highlighted by the yellow triangles).

contribute to Γ_{MR}. Before yielding ($\varepsilon_{max} < 3$), the contribution of matrix is negligible, so Γ_{MR} equals to $\Gamma_{microgel}$; after yielding ($\varepsilon_{max} > 3$), the matrix plays a comparable role as the microgel due to the swelling release of the matrix phase or the partial pull-out of PAAm chains from the microgel phase, which results in $\Gamma_{MR} < \Gamma_{microgel}$.

Combining with the mechanical relationship of $\sigma \sim \varepsilon$ and $d\sigma/d\varepsilon \sim \varepsilon$ as shown in Figure 1, we are able to elaborate the fracture picture of MR gels under uniaxial tension from a molecular point of view. In the elastic region ($0 < \varepsilon < 1$), σ increases with ε without any fracture in microgels, and the tangent modulus $d\sigma/d\varepsilon$ increases with ε due to the strain hardening of the stretched PNaAMPS chains. In the preyielding region ($1 < \varepsilon < 3$), the stress–strain curve gradually becomes nonlinear and starts to exhibit significant hysteresis in the loading–unloading cycle,[30] and $d\sigma/d\varepsilon$ decreases fast with ε, which result from the fracture of the short PNaAMPS chains in the axial direction of microgels. In the yielding region ($3 < \varepsilon < 7$), a slight increase in σ gives rise to a large ε, and $d\sigma/d\varepsilon$ experiences a U-shaped change, as a result of the mutual contributions of the further fracture in the axial long chains and the transverse short chains of microgels and the strain hardening of the PAAm chains. In the hardening region ($\varepsilon > 7$), the stress–strain curve starts to stiffen and climbs up until the ultimate failure, and $d\sigma/d\varepsilon$ increases linearly as ε, as a result of the fracture in the transverse long chains of microgels and the strain hardening of the PAAm chains. Thus, combining the macroscopic stress–strain curve with microscopic morphology analysis of microgels in the reswollen MR gels, we can elucidate the intrinsic correlation between the mechanical response of MR gels and the internal fracture of microgels.

Size Effect of Microgels. Although the microgels in MR gels have a diameter distribution from 2 to 11 μm in their initial state ($\varepsilon_{max} = 0$),[29] the above discussion only gives the average information about the fracture of microgels during the uniaxial tensile process, ignoring the size effect of microgels. What is the role the wide size distribution on earth plays in the nonlinear fracture process of MR gels under uniaxial tension? Next, we will pay much attention to the distribution of the swelling anisotropy γ of each individual microgel under the various ε_{max} to investigate the size effect of microgels.

Figure 4 shows the dependence of the swelling anisotropy γ of each individual microgel on its equivalent diameter d at different ε_{max}. According to the slope sign of the fitting lines, we

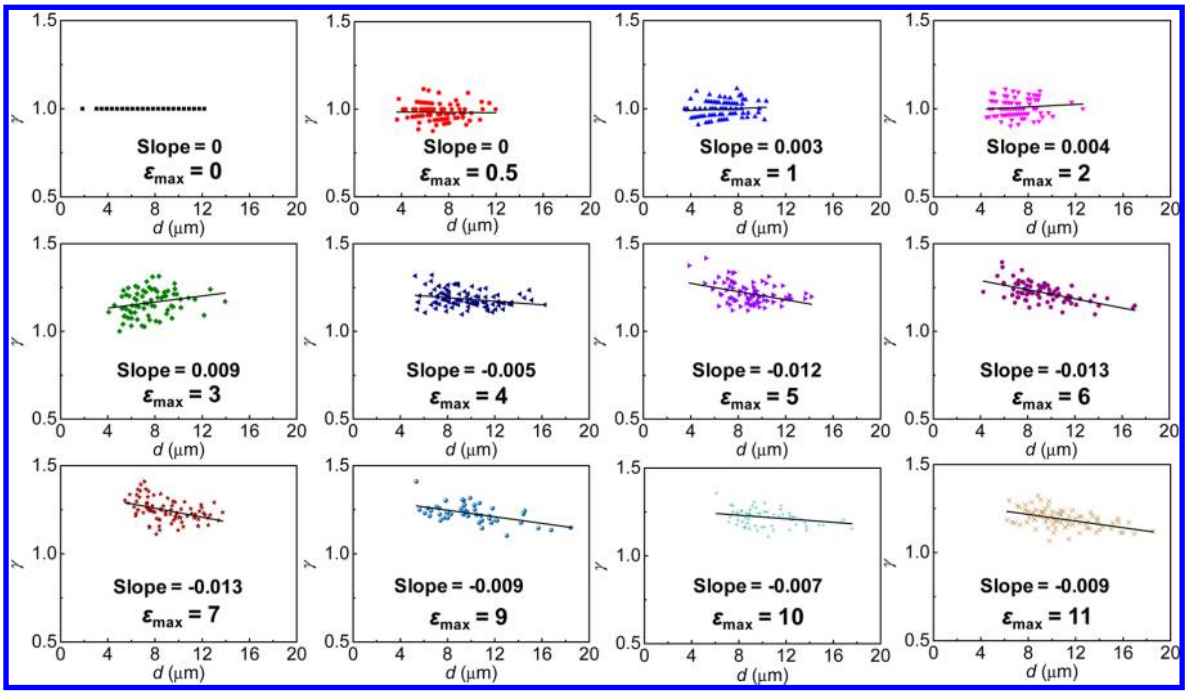

Figure 4. Dependence of swelling anisotropy γ of each individual microgel on its equivalent diameter d for MR gels undergoing different maximum strains ε_{max}. 100 microgels were statistically analyzed for each sample. The solid lines are the linear fits to the data in all the graphs, and the slopes of the lines indicate the fracture extent of microgels upon their d after experiencing a certain strain ε_{max}.

dx.doi.org/10.1021/ma5008545 | Macromolecules XXXX, XXX, XXX–XXX

find a subtle phenomenon that large microgels have larger γ than small ones below the yield point ($\varepsilon_{max} < 3$); on the contrary, small microgels have larger γ above the yield point ($\varepsilon_{max} > 3$), which implies that the fracture of microgels is size-dependent. Figure 5 shows the $\gamma-\varepsilon_{max}$ relationships of three

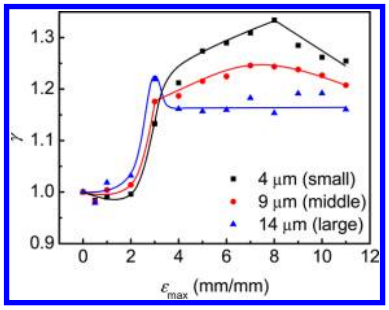

Figure 5. Dependence of swelling anisotropy γ of three kinds of microgels with different diameter on maximum strain ε_{max} for MR gels. The microgels with the diameter of 4, 9, and 14 μm are chosen to represent small, middle, and large microgels, respectively. All the γ values were calculated from the fitting lines in Figure 4.

kinds of microgels with the diameter of 4, 9, and 14 μm as a representation of small, middle, and large microgels, respectively. Middle microgels show the similar variation trend of γ to the mean swelling anisotropy $\Gamma_{microgel}$ shown in Figure 2e, also including the four regions mentioned in Figure 1, which indicates the major middle microgels dominate the macroscopic mechanical response of MR gels. Large microgels show the larger γ than small and middle ones before the yield point ($\varepsilon_{max} < 3$); above the yield point, γ decreases sharply and tends to reach a constant. These results indicate that the dominant fracture occurs in the axial chains of large microgels before yielding, while after yielding it occurs in the transverse chains. Small microgels show the smallest γ at $\varepsilon_{max} < 3$, and γ increases persistently until $\varepsilon_{max} = 8$, and finally decreases with ε_{max}. It seems more reasonable to divide the four fracture regions of small microgels into $0 < \varepsilon_{max} < 2$, $2 < \varepsilon_{max} < 4$, $4 < \varepsilon_{max} < 8$, and $\varepsilon_{max} > 8$, all of which has a lag in ε_{max} of 1 behind that of middle microgels. Moreover, the ultimate γ values of all these three kinds of microgels are larger than 1, suggesting more chains are fractured in the axial direction than in the transverse one; the ultimate γ value is smallest for large microgels, indicating the highest fracture efficiency in the chain rupture for large microgels. Figure 5 clearly reveals the size-dependent anisotropic fracture of microgels in the whole tensile process; that is, large microgels fracture *prior to* small ones and own the higher fracture efficiency in the chain rupture. This size-dependent fracture process of microgels should be the reason why MR gels do not exhibit an obvious yield point in the stress–strain curve as shown in Figure 1.

Why do large microgels fracture prior to small ones and own the higher fracture efficiency in the chain rupture although they have the same composition? In essence, both the wide size distribution and the heterogeneous spatial distribution of microgels in MR gels are responsible for the size effect on the fracture of microgels. We consider that large microgels have a higher probability to be close to the neighboring microgels than the smaller ones. Because of this, strain hardening of the soft PAAm matrix in the gap near large microgels occurs early, which causes preferential breaking of the brittle network of large microgels, as schematically illustrated in Figure 6a. Figure 6b shows a microscopic optical image of a MR gel being

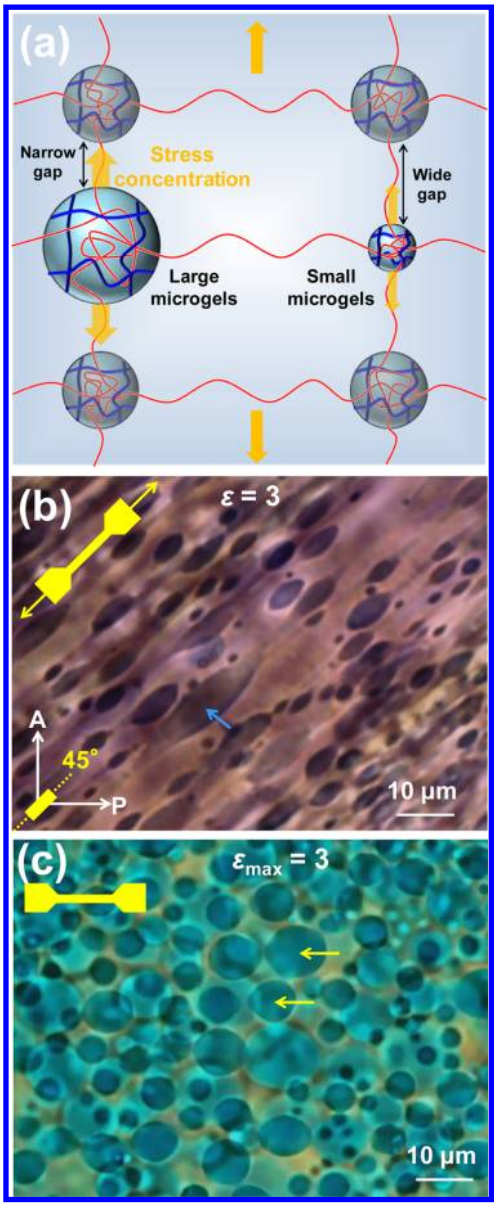

Figure 6. (a) Schematic illustration of different microenvironments of large microgels and small microgels in MR gels. For simplicity, the PAAm network matrix in the gap between microgels is only shown by few typical chains in the figure. (b) In-situ observation of microgel morphology in MR gels at the yield strain $\varepsilon = 3$ under the polarizing optical microscope, equipped with the crossed polarizers and the 530 nm tint plate. The sample was stretched 45° against the polarizers. The blue arrow is to highlight one deformed large microgel with a spindle-like shape. (c) Microgel morphology observation of reswollen MR gels experiencing the maximum strain $\varepsilon_{max} = 3$ under an optical microscope. The yellow arrows highlight the microgels with irregular shape, affected by their neighboring microgels. Part b is a reproduction of Figure 7a in the literature.[30]

stretched at the yield strain, in which large microgels significantly deformed into spindle-like shape are observed, the evidence that highly concentrated stress exists at the two poles of the large microgel. Moreover, these microgels form irregular shape in the corresponding reswelling state, affected by their neighboring microgels, as shown in Figure 6c. These results demonstrate that the fracture of microgels is strongly influenced by the wide size distribution and the heterogeneous spatial distribution. The size-dependent fracture process, that

dx.doi.org/10.1021/ma5008545 | *Macromolecules* XXXX, XXX, XXX–XXX

the large microgels fracture prior to small ones and own the higher fracture efficiency in the chain rupture, is attributed to the stress concentration effect on large microgels. This conclusion further supports our previously published argument that the stress concentration effect around microgels result in the higher fracture efficiency of MR gels than conventional DN gels.[30]

For the conventional PAMPS/PAAm DN hydrogels, whether or not the heterogeneity of the first PAMPS network plays an intrinsic role for the high strength and toughness of DN gels had been a puzzle.[10] One recent study on a novel Tetra-PEG/PAAm DN gel, where the first network is homogeneous, clearly elucidates that the heterogeneity of the first network is not essential for the toughening mechanism of conventional DN gels.[34] In fact, the heterogenoues first network first experiences a homogenization process before yielding, in which the preferential fracture occurs in the axial short chains of the first network.[8] The second network redistributes the stress through entanglement effects to avoid crack propagation. This result suggests that a homogeneous stress distribution is important for the steady fracture of DN gels. In the case of MR gels, the large microgels fracture prior to the small ones and subject to a larger degree of chain rupture, which is also a homogenization process. Although having completely different mesoscale structure between DN gels and MR gels, they have a common fracture picture; that is, they achieve a relatively homogeneous stress distribution through preferentially fracturing the zones of stress concentration.

Tensile Fracture Surface of MR Gels. Figure 7 shows the morphology of microgels in a reswollen MR gel after ultimate failure. Several fragmentary microgels are observed at the fractured surface, indicating that the catastrophic crack propagates through the PAAm matrix and the soften microgels with no detour. On the other hand, the microgels far away from the fractured surface still keep their integrity even after the sample failure. This suggests that some long PNaAMPS chains still remain to maintain the shape of microgels, although they suffer significant internal fracture in both the axial direction and the transverse direction during the uniaxial elongation.

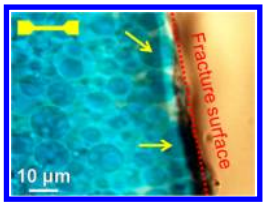

Figure 7. Morphology observation of a reswollen MR gel after ultimate failure. The red dotted line represents the fractured surface, and the yellow arrows highlight the microgels fractured into small pieces.

CONCLUSIONS

We have synthesized a kind of strong and tough MR hydrogel with a novel two-phase composite structure, where the disperse phase is viewed as the rigid DN microgels and the continuous phase is the soft PAAm matrix. In MR gels, the densely cross-linked PNaAMPS microgels act as multifunctional physical cross-linkers to confine the swelling of sparsely cross-linked PAAm matrix through mutual entanglement. The entanglement between the PAAm matrix phase and the microgels phase plays a crucial role in stress transmission. According to the mechanical relationship $d\sigma/d\varepsilon \sim \varepsilon$, the tensile stress−strain curve $\sigma \sim \varepsilon$ of MR gels could be divided into four regions, as elastic region ($0 < \varepsilon < 1$), preyielding region ($1 < \varepsilon < 3$), yielding region ($3 < \varepsilon < 7$), and strain hardening region ($\varepsilon > 7$). On the basis of the quantitative morphology analysis of the swelling anisotropy Γ of microgels in the reswollen MR gels after prestretching, we clarify the fracture process of MR gels under the uniaxial tension from a molecular point of view. That is, no fracture occurs in the elastic region ($0 < \varepsilon < 1$), and predominant fracture of microgels occurs in the order as follows: the axial short chains ($1 < \varepsilon < 3$), the axial long chains and the transverse short chains ($3 < \varepsilon < 7$), and the transverse long chains ($\varepsilon > 7$). Further, we successfully elucidate the intrinsic correlation between the macroscopic mechanical response of MR gels and the microscopic internal fracture of microgels. Moreover, at each stage of the tensile process, large microgels always fracture prior to small ones and own the higher fracture efficiency in the chain rupture. This size effect is attributed to the stress concentration effect on large microgels induced by the narrow gap near large microgels. The absence of the distinct yield point in the stress−strain mechanical response of MR gels is also ascribed to this size-dependent fracture process. The clear fracture picture of MR gels under uniaxial tension, in turn, will aid us in building physical models to describe fracture behaviors such as the Mullins effect in loading−unloading hysteresis cycle as well as designing better products with tunable performance to meet various practical requirements.

AUTHOR INFORMATION

Corresponding Author

*E-mail: gong@mail.sci.hokudai.ac.jp (J.P.G.).

Notes

The authors declare no competing financial interest.

ACKNOWLEDGMENTS

We thank Dr. C. Creton of ESPCI, France, for beneficial discussions. This research was financially supported by a Grant-in-Aid for Scientific Research (S) (No. 124225006) from Japan Society for the Promotion of Science (JSPS).

REFERENCES

(1) Gong, J. P.; Katsuyama, Y.; Kurokawa, T.; Osada, Y. *Adv. Mater.* **2003**, *15*, 1155.
(2) Okumura, Y.; Ito, K. *Adv. Mater.* **2001**, *13*, 485.
(3) Haraguchi, K.; Takehisa, T. *Adv. Mater.* **2002**, *14*, 1120.
(4) Fung, Y. C. *Biomechanics: Mechanical Properties of Living Tissues*, 2nd ed.; Springer-Verlag: New York, 1993.
(5) Taylor, D.; O'Mara, N.; Ryan, E.; Takaza, M.; Simms, C. *J. Mech. Behav. Biomed. Mater.* **2012**, *6*, 139.
(6) Naficy, S.; Brown, H. R.; Razal, J. M.; Spinks, G. M.; Whitten, P. G. *Aust. J. Chem.* **2011**, *64*, 1007.
(7) Na, Y.-H.; Tanaka, Y.; Kawauchi, Y.; Furukawa, H.; Sumiyoshi, T.; Gong, J. P.; Osada, Y. *Macromolecules* **2006**, *39*, 4641.
(8) Webber, R. E.; Creton, C.; Brown, H. R.; Gong, J. P. *Macromolecules* **2007**, *40*, 2919.
(9) Yu, Q. M.; Tanaka, Y.; Furukawa, H.; Kurokawa, T.; Gong, J. P. *Macromolecules* **2009**, *42*, 3852.
(10) Gong, J. P. *Soft Matter* **2010**, *6*, 2583.
(11) Ahmed, S.; Nakajima, T.; Kurokawa, T.; Haque, M. A.; Gong, J. P. *Polymer* **2014**, *55*, 914.
(12) Haque, M. A.; Kurokawa, T.; Kamita, G.; Gong, J. P. *Macromolecules* **2011**, *44*, 8916.

(13) Saito, J.; Furukawa, H.; Kurokawa, T.; Kuwabara, R.; Kuroda, S.; Hu, J.; Tanaka, Y.; Gong, J. P.; Kitamura, N.; Yasuda, K. *Polym. Chem.* **2011**, *2*, 575.
(14) Nakajima, T.; Sato, H.; Zhao, Y.; Kawahara, S.; Kurokawa, T.; Sugahara, K.; Gong, J. P. *Adv. Funct. Mater.* **2012**, *22*, 4426.
(15) Suekama, C. T.; Hu, J.; Kurokawa, T.; Gong, J. P. *ACS Macro Lett.* **2013**, *2*, 137.
(16) Yin, H. Y.; Akasaki, T.; Sun, T. L.; Nakajima, T.; Kurokawa, T.; Nonoyama, T.; Taira, T.; Saruwatari, Y.; Gong, J. P. *J. Mater. Chem. B* **2013**, *1*, 3685.
(17) Sun, T. L.; Kurokawa, T.; Kuroda, S.; Ihsan, A. B.; Akasaki, T.; Sato, K.; Haque, M. A.; Nakajima, T.; Gong, J. P. *Nat. Mater.* **2013**, *12*, 932.
(18) Zhao, Y.; Nakajima, T.; Yang, J. J.; Kurokawa, T.; Liu, J.; Lu, J. S.; Mizumoto, S.; Sugahara, K.; Kitamura, N.; Yasuda, K.; Daniels, A. U. D.; Gong, J. P. *Adv. Mater.* **2014**, *26*, 436.
(19) Waters, D. J.; Engberg, K.; Parke-Houben, R.; Hartmann, L.; Ta, C. N.; Toney, M. F.; Frank, C. W. *Macromolecules* **2010**, *43*, 6861.
(20) Sakai, T.; Matsunaga, T.; Yamamoto, Y.; Ito, C.; Yoshida, R.; Suzuki, S.; Sasaki, N.; Shibayama, M. *Macromolecules* **2008**, *41*, 5379.
(21) Kaneko, T.; Tanaka, S.; Ogura, A.; Akashi, M. *Macromolecules* **2005**, *38*, 4861.
(22) Huang, T.; Xu, H. G.; Jiao, K. X.; Zhu, L. P.; Brown, H. R.; Wang, H. L. *Adv. Mater.* **2007**, *19*, 1622.
(23) Lin, W. C.; Fan, W.; Marcellan, A.; Hourdet, D.; Creton, C. *Macromolecules* **2010**, *43*, 2554.
(24) Henderson, K. J.; Zhou, T. C.; Otim, K. J.; Shull, K. R. *Macromolecules* **2010**, *43*, 6193.
(25) Wang, Q.; Mynar, J.; Yoshida, M.; Lee, E.; Lee, M.; Okuro, K.; Kinbara, K.; Aida, T. *Nature* **2010**, *463*, 339.
(26) Sun, J. Y.; Zhao, X.; Illeperuma, W. R. K.; Chaudhuri, O.; Oh, K. H.; Mooney, D. J.; Vlassak, J. J.; Suo, Z. *Nature* **2012**, *489*, 133.
(27) Chen, Q.; Zhu, L.; Zhao, C.; Wang, Q.; Zheng, J. *Adv. Mater.* **2013**, *25*, 4171.
(28) Hu, J.; Hiwatashi, K.; Kurokawa, T.; Liang, S. M.; Wu, Z. L.; Gong, J. P. *Macromolecules* **2011**, *44*, 7775.
(29) Hu, J.; Kurokawa, T.; Hiwatashi, K.; Nakajima, T.; Wu, Z. L.; Liang, S. M.; Gong, J. P. *Macromolecules* **2012**, *45*, 5218.
(30) Hu, J.; Kurokawa, T.; Nakajima, T.; Sun, T. L.; Suekama, T.; Wu, Z. L.; Liang, S. M.; Gong, J. P. *Macromolecules* **2012**, *45*, 9445.
(31) Shin, H.; Olsen, B. D.; Khademhosseini, A. *J. Mater. Chem. B* **2014**, *2*, 2508.
(32) Nakajima, T.; Kurokawa, T.; Ahmed, S.; Wu, W. L.; Gong, J. P. *Soft Matter* **2013**, *9*, 1955.
(33) Tominaga, T.; Tirumala, V. R.; Lin, E. K.; Gong, J. P.; Furukawa, H.; Osada, Y.; Wu, W. L. *Polymer* **2007**, *48*, 7449.
(34) Nakajima, T.; Fukuda, Y.; Kurokawa, T.; Sakai, T.; Chung, U.; Gong, J. P. *ACS Macro Lett.* **2013**, *2*, 518.